Chapter 6
Strain Engineering of 2D Materials

When bulk structures are thinned down to their monolayers, degree of orbital interactions, mechanical properties and electronic band dispersion of the crystal structure become highly sensitive to the amount of applied strain. The source of strain on the ultra-thin lattice structure can be (1) an external device or a flexible substrate that can stretch or compress the structure, (2) the lattice mismatch between the layer and neighboring layers or (3) stress induced by STM or AFM tip.

6.1 MoS$_2$

Among the ultra-thin TMDs MoS$_2$ is the most studied one due to its easy synthesis, semiconducting nature, atomically perfect surface structure and abundance. It has also been shown experimentally and computationally that elastic strain is a viable agent for creating a continuously varying bandgap profile in an initially homogeneous, atomically thin single layer MoS$_2$ which is highly desirable for its use in photovoltaics, photocatalysis and photodetection (Feng et al. 2012). As shown by Feng et al. the electronic bandgap of the single layer structure can be tuned significantly and reversibly upon biaxial strain (see Fig. 6.1). Therefore, it was also shown that single layer MoS$_2$ based photovoltaic devices can capture broad range of the solar spectrum upon application of strain. Moreover, these devices can concentrate excitons and charge carriers in desired domains of the crystal structure.

Another device example is optoelectronic crystal of artificial atoms in strain-textured MoS$_2$ (Li et al. 2015). This was achieved by transferring as-grown MoS$_2$ sheet onto assembled SiO$_2$ nanocones and then soaking it in ethylene glycol to remove the trapped air bubbles while optimizing the strain (see Fig. 6.2). The evaporation of ethylene glycol from the interface generates capillary force that applies local strain to the MoS$_2$ sheet. It was shown that a synthetic superlattice of
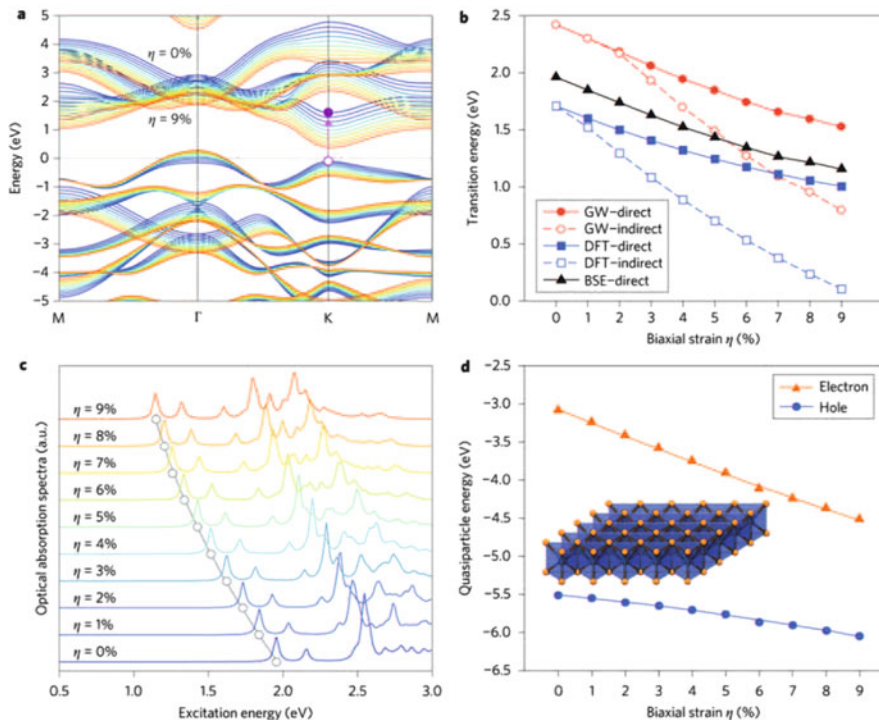
Fig. 6.1 (**a**) Strain dependent electronic band structure of monolayer MoS_2 under different biaxial strains from 0 (*blue line*) to 9 % (*red line*). (**b**) Direct and indirect bandgaps under different biaxial strains calculated using DFT and GW. Strain-dependent (**c**) absorption spectra and (**d**) quasi-particle energy of electron and hole. Adapted from Feng et al. (2012)

capillary-pressure-induced nanoindentation of monolayer molybdenum disulphide forms an optoelectronic crystal capable of broadband light absorption which covers the entire visible wavelength and most intensive wavelengths of the solar spectrum. It was also discussed by Li et al. that such two-dimensional semiconductors with spatially textured band gaps represent a new class of materials, which may find applications in next-generation optoelectronics or photovoltaics.

6.2   MoSe$_2$

Lattice vibrations of single layer $MoSe_2$ crystal that has the D_{3h} point group symmetry can be characterized by nine phonon branches including three acoustic and six optical branches. While LA and TA acoustic branches have linear dispersion, the frequency of the out of plane flexural (ZA) mode has a quadratic dispersion in the vicinity of q = 0. Decomposition of optical vibrations at the zone center reveals that
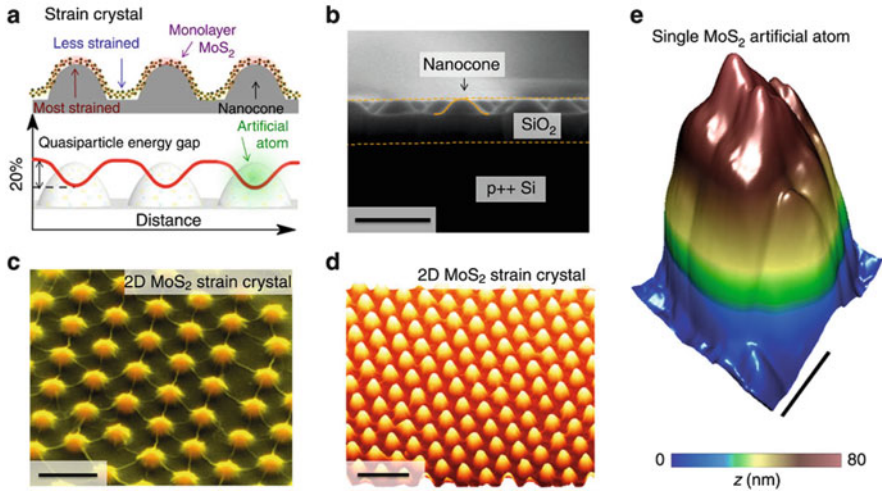
Fig. 6.2 (**a**) Schematic of strained MoS$_2$ indented by SiO$_2$ nanocones, where the regions on the tips of nanocones exhibit highest tensile strain while the areas between nanocones are less strained. (**b**) Cross-sectional scanning electron microscopy (SEM) image of the nanocone substrate. *Solid curve* delineates the nanocone shape. Scale bar is 500 nm. (**c**) Tilted false-color SEM image of the 2D strained MoS$_2$ crystal defined by the nanocone array. Scale bar is 500 nm. (**d**) AFM topography of the 2D MoS$_2$ strain crystal. Scale bar is 1 m. (**e**) STM topography of a single "artificial atom" building block within the crystal. Scale bar is 100 nm. Adapted from Li et al. (2015)

there are 2E$''$, 2E$'$, A$_1'$ and A$_2''$ modes. While atoms have in-plane motion in E modes they move in out-of-plane direction in A modes. Among these 6 optical branches only 2E$''$, 2E$'$ and A$_1'$ modes are Raman-active and measurable in Raman intensity measurements. Ab initio calculations show that the lattice dynamics of single layer MoSe$_2$ is quite sensitive to the applied strain (Horzum et al. 2013). As shown in Fig. 6.3 while the phonon branches having in-plane motion symmetry are softened significantly, out-of-plane Raman-active phonon branch are almost insensitive to applied biaxial strain.

Horzum et al. also showed that not only vibrational properties but also electronic characteristics of the monolayer MoSe$_2$ can be tuned by applied biaxial strain. As presented in Fig. 6.4, when the tensile strain is increased, electronic states around the *K* symmetry point rapidly shift down to lower energies and the shift in other regions of the Brillouin Zone is quite slower. Therefore, after a certain strain value (3 %) monolayer MoSe$_2$ which is a direct bandgap semiconductor in its ground state becomes an indirect semiconductor.
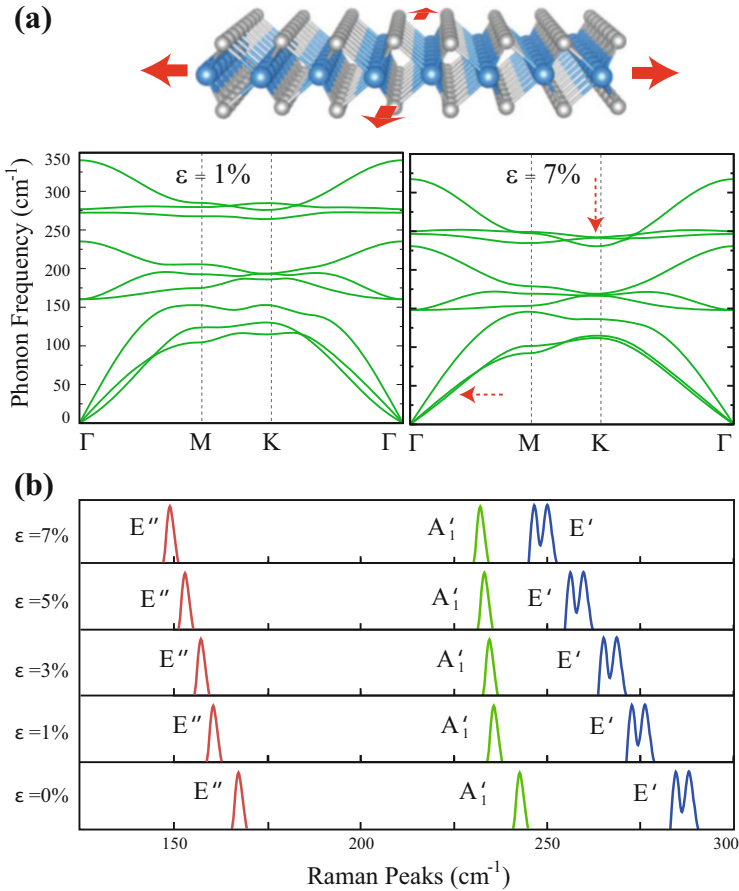
Fig. 6.3 Strain-dependent phonon dispersion and frequency shift in single layer $MoSe_2$. (a) Phonon dispersions for 1% and 7% strained single layer $MoSe_2$. (b) Evolution of the Raman-active modes as a function of applied strain. Adapted from Horzum et al. (2013)

6.3 WSe_2

Following theoretical findings on single layer $MoSe_2$, one can expect similar behavior in electronic and vibrational characteristics of single layer WSe_2. Both structures have the same crystal symmetry and both Mo and W atoms have the same chemical characteristics. However, Sahin et al. reported some unique features, that do not exist in other TMDs, in the vibrational spectrum of WSe_2 (Sahin et al. 2013). As shown in Fig. 6.5a, experimentally observed most prominent Raman peak is located at $252 \, cm^{-1}$. While other semiconducting TMDs are characterized by well-separated E_g and A_g Raman peaks, bulk WSe_2 has just one prominent peak in its spectrum. Experiments revealed that there is an additional Raman-active mode
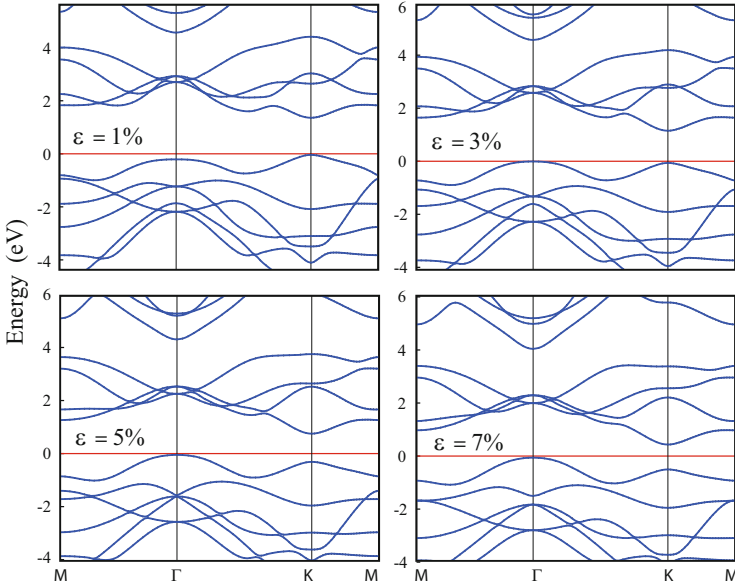
Fig. 6.4 Evolution of the electronic band structure of single layer MoSe$_2$ upon biaxial strain. Valence band edge is set to zero. Adapted from Horzum et al. (2013)

which is only visible when the structure becomes ultra-thin. Deeper understanding of this anomaly was provided by theoretical calculations performed (Sahin et al. 2013). As shown in Fig. 6.5b, in theoretically observed phonon dispersion of the bulk WSe$_2$ well-separated E$_g$ and A$_g$ Raman-active modes have an "accidental degeneracy". Furthermore, it was also seen that bilayer and monolayer crystal structures of WSe$_2$ possess the same unique feature (see Fig. 6.5d–e).

Then, the question is why the accidental degeneracy, which is a characteristics of WSe$_2$, is broken in experiments. Since the secondary Raman-active peak (shoulder of the most prominent peak) in spectrum is visible only in ultra-thin crystals, an explanation based on the substrate-induced strain is quite reasonable. As shown in Fig. 6.6, while the biaxial strain on monolayer crystal structure has no influence on the accidentally degenerate modes, these phonon branches become well-separated upon application of mild uniaxial strain. The response of the crystal structure against tensile strain is found to be the same in both zigzag and armchair directions. Therefore, one can conclude the reason of broken accidentally degeneracy as the substrate-induced uniaxial strain.

6.4 ReSe$_2$

In addition to large amount of research effort on dichalcogenides of molybdenum and tungsten (group-VI TMDs), recent studies have also focused on crystal
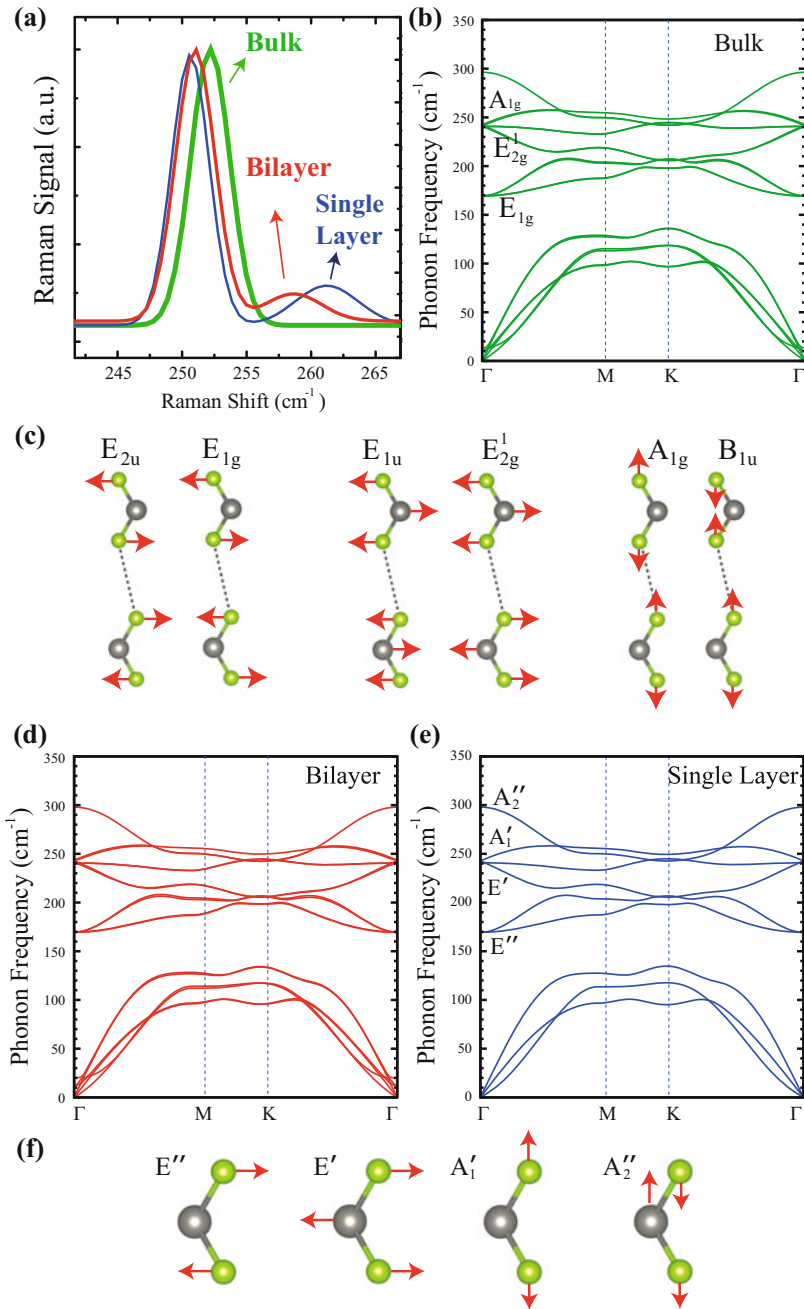
Fig. 6.5 (a) Experimentally observed Raman spectrum bulk,bilayer and monolayer WSe₂.
(b) Calculated phonon dispersion and (c) atomic displacements of the bulk structure. Phonon
dispersion of (d) bilayer and (e) monolayer structure and (f) atomic displacements in monolayer
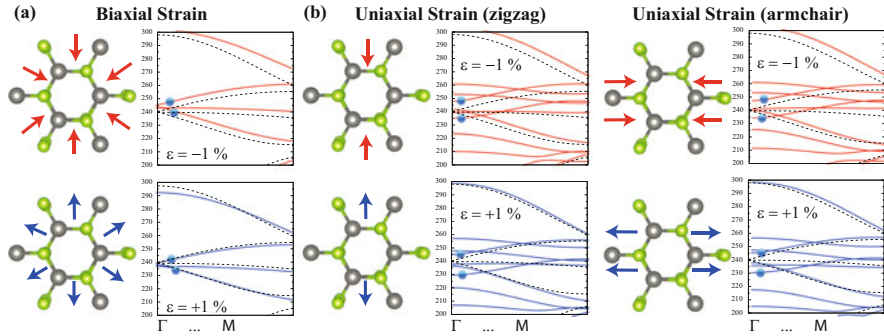structure. Adapted from Sahin et al. (2013)

Fig. 6.6 Strain-dependent phonon dispersion and frequency shift in single layer WSe$_2$. Adapted from Sahin et al. (2013)
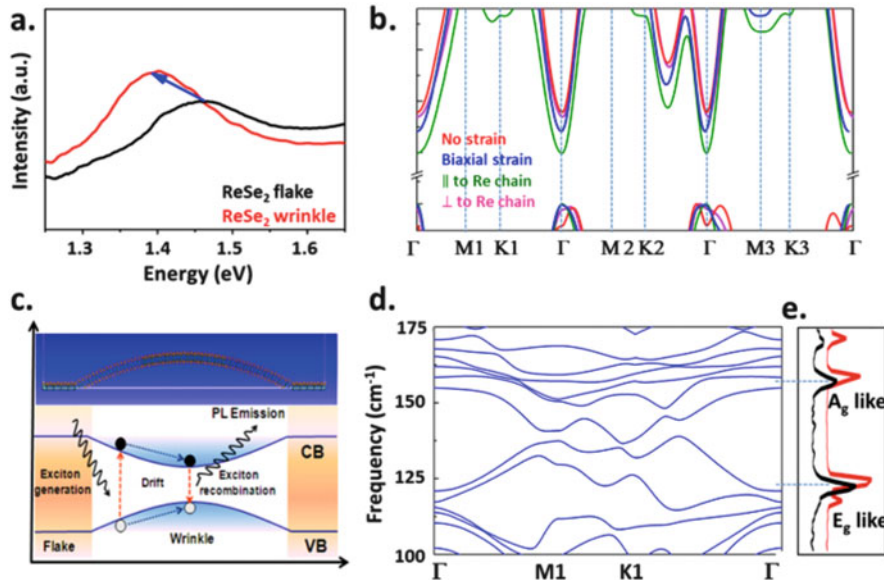

Fig. 6.7 Strain-dependent phonon dispersion and frequency shift in single layer ReSe$_2$. Adapted from Yang et al. (2015)

structures of group-VII TMDs such as ReS$_2$ and ReSe$_2$ (Tongay et al. 2014; Yang et al. 2015). Differing from other TMDs extra electron in the d-orbitals of Rhenium atom leads to large differences. For example, ReS$_2$ and ReSe$_2$ lack dimensional-crossover-driven indirect-to-direct gap transition but possess strong in-plane anisotropy and a rich Raman spectrum.

In a recent study, Yang et al. showed that local strain induced by generation of wrinkles reduces the optical gap as evidenced by red-shifted photoluminescence peak (Fig. 6.7a–c). It was also shown that locally-strained domain is not only
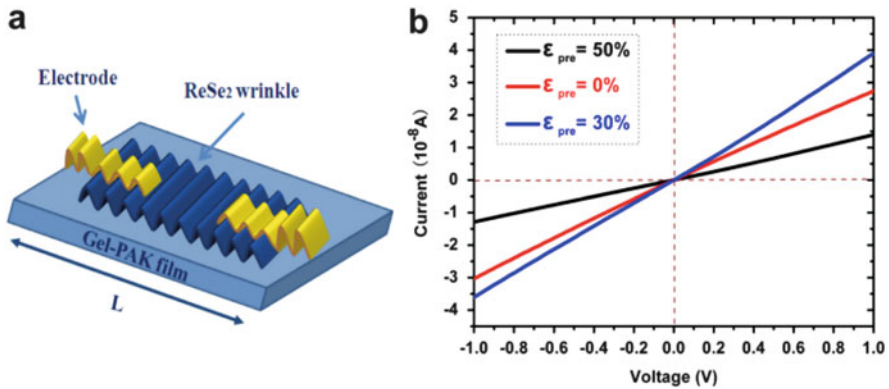
Fig. 6.8 Electrical characterization on strained ReSe$_2$. (**a**) Schematic drawing of a two-terminal ReSe$_2$ wrinkles device. (**b**) I-V curves of a two terminal ReSe$_2$ wrinkles device under different prestrain. Adapted from Yang et al. (2015)

provides a enhanced PL intensity but also a suitable playground for exciton recombination (Yang et al. 2015). In addition, theoretical calculations, shown in Fig. 6.7b, revealed that while the effect of local strain along the direction perpendicular to Re-Re dimers is ignorable, strain applied along the direction parallel to the dimers significantly alters the band gap. It was also experimentally demonstrated that formation of wrinkles may also leads to the presence of local magnetism. Furthermore, locally wrinkled domains in ReSe$_2$ have also strain-tunable I-V characteristics as shown in Fig. 6.8.

6.5   Black Phosphorus

Another promising material in the family of ultra-thin crystal structures is phosphorene (black phosphorus). Structural stability, anisotropic structural properties, a high on-current, a high hole field-effect mobility, and a high on/off ratio in few layer phosphorene FETs make black phosphorus suitable for various optoelectronic nanoscale device applications. Buscema et al. demonstrated that black phosphorus is an appealing candidate for tunable photodetection applications due its unique properties such as (1) FETs allowing for ambipolar operation in the dark state and (2) broadband (from the visible region up to 940 nm) with fast detection (rise time of about 1 ms) when illuminated (Buscema et al. 2014).

In addition, strain dependent electronic, quantum transport and optical properties of black phosphorus were investigated by a recent theoretical study (Horzum et al. 2014). As shown in Fig. 6.9, single layer phosphorus has different responses against compressive and tensile strain. While tensile strain has no significant effect on the electronic structure, energy bandgap is quite sensitive to the compressive strain. It is
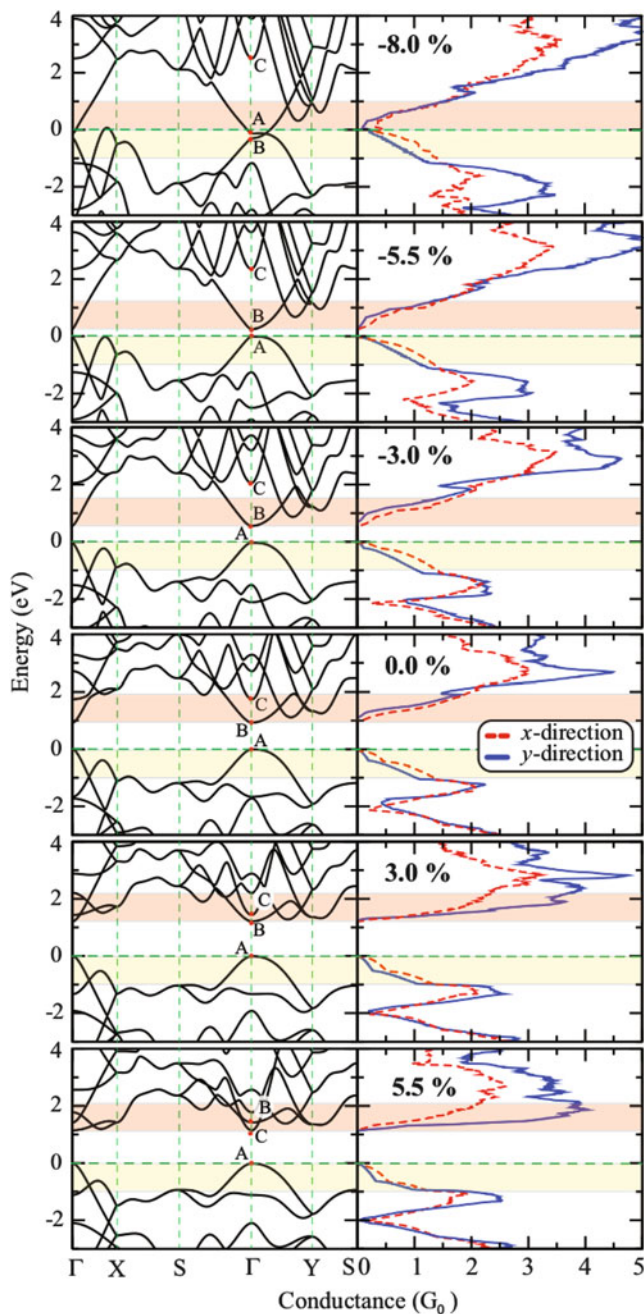
Fig. 6.9 Evolution of electronic band dispersion and conductance of single-layer phosphorene under biaxial strain. A, B, and C mark the top of the valence band, bottom of the conduction band, and the second lowest conduction band at the Γ point, respectively. *Shaded regions* depict the upper part of the valence and lower part of the conduction bands

also seen that while the states at the valence band edge are not affected by the strain, conduction band edges, especially around the Γ point, rapidly shifts down in energy space. Therefore, such behavior results in metallicity after 6 % compressive strain. However, rapid shift in C band edge upon tensile strain may also lead to metallicity in monolayer phosphorus. Furthermore, stemming from the structural anisotropy, black phosphorus shows different quantum transport characteristics in armchair and zigzag directions.

To conclude, graphene, silicene and similar ultra-thin crystals are quite promising building blocks for a wide range of strain-based device applications such as strain sensors, stretchable electrodes, flexible field-effect transistors, electromechanical, piezoelectric devices.

References

Buscema, M., Groenendijk, D.J., Steele, G.A., van der Zant, H.S.J., Castellanos-Gomez, A.: Photovoltaic effect in few-layer black phosphorus PN junctions defined by local electrostatic gating. Nat. Commun. **5** (2014). doi:10.1038/ncomms5651

Feng, J., Qian, X., Huang, C.W., Li, J.: Strain-engineered artificial atom as a broad-spectrum solar energy funnel. Nat. Photonics **6**, 866–872 (2012)

Horzum, S., Sahin, H., Cahangirov, S., Cudazzo, P., Rubio, A., Serin, T., Peeters, F.M.: Phonon softening and direct to indirect band gap crossover in strained single-layer mose$_2$. Phys. Rev. B **87**, 125415 (2013)

Horzum, S., Çakır, D., Suh, J., Tongay, S., Huang, Y.S., Ho, C.H., Wu, J., Sahin, H., Peeters, F.M.: Formation and stability of point defects in monolayer rhenium disulfide. Phys. Rev. B **89**, 155433 (2014)

Li, H., Contryman, A.W., Qian, X., Ardakani, S.M., Gong, Y., Wang, X., Weisse, J.M., Lee, C.H., Zhao, J., Ajayan, P.M., Li, J., Manoharan, H.C., Zheng, X.: Optoelectronic crystal of artificial atoms in strain-textured molybdenum disulphide. Nat. Commun. **6** (2015). doi:10.1038/ncomms8381

Sahin, H., Tongay, S., Horzum, S., Fan, W., Zhou, J., Li, J., Wu, J., Peeters, F.M.: Anomalous raman spectra and thickness-dependent electronic properties of WSe$_2$. Phys. Rev. B **87**, 165409 (2013b)

Tongay, S., Sahin, H., Ko, C., Luce, A., Fan, W., Liu, K., Zhou, J., Huang, Y.S., Ho, C.H., Yan, J., Ogletree, D.F., Aloni, S., Ji, J., Li, S., Li, J., Peeters, F.M., Wu, J.: Monolayer behaviour in bulk ReS2 due to electronic and vibrational decoupling. Nat. Commun. **5** (2014). doi:10.1038/ncomms4252

Yang, S., Wang, C., Sahin, H., Chen, H., Li, Y., Li, S.S., Suslu, A., Peeters, F.M., Liu, Q., Li, J., Tongay, S.: Tuning the optical, magnetic, and electrical properties of rese2 by nanoscale strain engineering. Nano Lett. **15**, 1660–1666 (2015)